Monodromy and chaos for condensed bosons in optical lattices

Geva Arwas[1,2] and Doron Cohen[1]
[1]*Department of Physics, Ben-Gurion University of the Negev, Beer-Sheva 84105, Israel*
[2]*Department of Physics of Complex Systems, Weizmann Institute of Science, Rehovot 7610001, Israel*

(Received 23 September 2018; published 25 February 2019)

We introduce a theory for the stability of a condensate in an optical lattice. We show that the understanding of the stability-to-ergodicity transition involves the fusion of *monodromy* and *chaos* theory. Specifically, the condensate can decay if a connected chaotic pathway to depletion is formed, which requires swap of separatrices in phase space.

DOI: 10.1103/PhysRevA.99.023625

I. INTRODUCTION

Ergodicity, as opposed to stability, is the threat that looms over the condensation of bosons in optical lattices. A major question of interest is whether an initial condensate is likely to be depleted. The simplest setup is the dimer, also known as the Bosonic Josephson junction [1–3], where condensation in the upper orbital can become unstable if the interaction exceeds a critical value. A more challenging setup is a ring lattice [4–8], where the particles are condensed into an excited momentum orbital. If such a flow state is metastable, it can be regarded as a mesoscopic version of superfluidity. It has been realized that the theory for this superfluidity requires analysis that goes beyond the traditional framework of Landau and Bogoliubov, because the underlying dynamics is largely chaotic [9,10].

The structure of the classical phase space is reflected in the quantum spectrum, and provides the key for the quantum-chaos theory of mesoscopic superfluity. In the present work we highlight the essential ingredient for the crossover from stability to ergodicity. We consider the minimal setup: a three-site ring. We show that the understanding of this transition involves the fusion of two major research themes: *monodromy* and *chaos*.

A. Monodromy

The dynamics of an integrable (nonchaotic) system, for a given value of the conserved constants of motion, can be described by a set of action-angle variables, that parametrize a torus in phase space. In systems with monodromy, they cannot be defined globally: due to the nontrivial topology of phase space, the action-angle variables cannot be identified in a continuous way in the parameter space that is formed by the conserved quantities [11,12]. Accordingly, it is impossible to describe the quantum spectrum by a global set of good quantum numbers [13,14]. Rather, the good quantum numbers (quantized "actions") that are implied by the Einstein-Brillouin-Keller (EBK) quantization scheme form a lattice that features a topological defect [15]. Such Hamiltonian monodromy is found in many physical systems, such as the spherical [13,16] and the swing-spring [17,18] pendula, spin-1 condensed bosons [19], the Dicke model [20], and even the hydrogen atom [21]. A dynamical manifestation of monodromy in a classical system has been recently demonstrated [22].

B. Chaos

The condensation of particles in a single orbital is a many-body coherent state. It can be represented in phase space as a Gaussian-like distribution that is supported by a stationary point (SP). If this SP is the minimum of the energy landscape, it is known as Landau energetic stability, and leads, for a clean ring, to the Landau criterion for superfluidity. More generally one has to find the Bogoliubov excitations ω_r of condensate. If some of the frequencies become complex, the SP is considered to be unstable. What we have demonstrated in previous work [5,10] was that this type of local stability analysis does not provide the required criteria for stability. Rather, in order to determine whether the system will ergodize, it is essential to study the global structure of phase space, and to take into account the role of chaos.

C. Connectivity

The major insight can be described schematically as follows. Let us regard the SP that supports the condensate as the *origin* of phase space. And let us regard the region that supports the completely depleted states as the *perimeter* of phase space. The crucial question is whether there is a dynamical pathway that leads from the origin to the perimeter. We have observed numerically in [10] that the formation of such pathway requires a swap of phase-space separatrices. But a theory for this swap transition has not been provided.

D. Outline

For pedagogical purposes we first consider the stability question for the dimer. Then we go to the trimer and write its Hamiltonian as the sum of integrable part $\mathcal{H}^{(0)}$, and additional terms $\mathcal{H}^{(\pm)}$ that induce the chaos. An example for the classical and quantum spectra is presented in Fig. 1. The spectra exhibit monodromy that we analyze in detail: the quantum monodromy is a reflection of the classical one. Then we explain how the spectrum is affected by changing a control parameter (detuning). In a hysteresis experiment [23] the detuning is determined by the rotation frequency of the device and the inter-

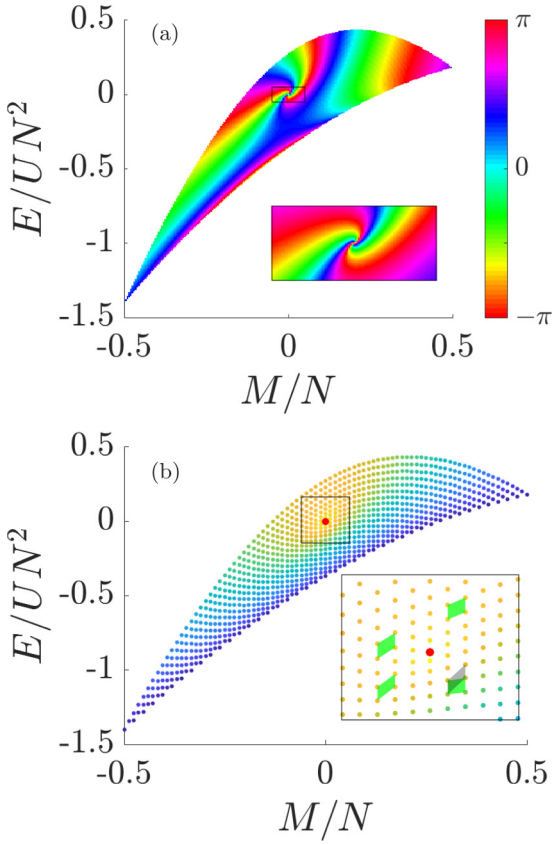

FIG. 1. Monodromy. The classical and quantum spectra of the Hamiltonian $\mathcal{H}^{(0)}$. This Hamiltonian has a constant of motion M, that describes the occupation imbalance of the $k \neq 0$ orbitals. In (a) each point represents an (M, E) torus in phase space, and the points are color coded by the value of a classical phase (β) that characterizes the torus. In (b) each point represents an $|M, E\rangle$ eigenstate of $N = 42$ particles, and the points are color coded by the expectation value of the variable n, which is the total occupation of the $k \neq 0$ orbitals. Yellow color ($n < N/8$) indicates a nearly coherent condensate, while blue implies a depleted eigenstate. In both panels $\mathcal{E}/NU \approx -1/4$ and $\mathcal{E}_\perp/NU \approx 1/2$. The inset provides a zoom that demonstrates the monodromy, a topological defect in the lattice arrangement of the spectrum.

action strength between the bosons. We provide a geometrical explanation for the *swap transition*, and clarify the role of chaos in the destabilization of the condensate. In the Summary section we point out the relevance of our study to the more general theme of thermalization in Bose-Hubbard chains.

II. MODEL

The Bose-Hubbard Hamiltonian (BHH) is a prototype model for cold atoms in optical lattices that has inspired state-of-the-art experiments [24,25], and has been proposed as a platform for quantum simulations. It describes a system of N bosons in L sites. The ring geometry in particular has attracted attention for atomtronic circuits [4]. Taking into account that N is a constant of motion, the system has $f = L-1$ degrees of freedoms. The simplest configuration is the dimer ($L = 2$), also known as the Bosonic Josephson junction. Our main interest is in the minimal nonintegrable configuration, which is the trimer ($L = 3$). Below we briefly refer to the dimer Hamiltonian, and then turn to discuss the trimer Hamiltonian. Further technical details about the latter are provided in Appendix A.

A. Dimer

The Hamiltonian of the dimer is

$$\mathcal{H}_{\rm dimer} = -\frac{K}{2}(a_2^\dagger a_1 + a_1^\dagger a_2) + \frac{U}{2}\sum_{j=1}^{2} a_j^\dagger a_j^\dagger a_j a_j, \qquad (1)$$

where K is the hopping frequency, U is the on-site interaction, The a_j and $a_j^\dagger$ are the Bosonic annihilation and creation operators. The total number of particles $N = \sum_j a_j^\dagger a_j$ is a constant of motion.

It is convenient to switch to orbital representation. One defines annihilation and creation operators b_k and $b_k^\dagger$, such that $b_\pm^\dagger = \frac{1}{\sqrt{2}}(a_1^\dagger \pm a_2^\dagger)$ creates bosons in the lower and upper orbitals. For the purpose of semiclassical treatment we define action-angle variables via

$$b_k \;=\; \sqrt{n_k}\, e^{i\varphi_k}. \qquad (2)$$

After dropping an N dependent constant the Hamiltonian takes the form

$$\mathcal{H}_{\rm dimer}(\tilde\varphi, \tilde n) \;=\; -\mathcal{E}\tilde n + \frac{U}{2}(N-\tilde n)\,\tilde n\,[1+\cos(2\tilde\varphi)], \qquad (3)$$

where $\tilde n = n_+$ is the occupation of the (+) orbital, and $\mathcal{E} = K$ is the detuning (energy difference between the orbitals). The angle $\tilde\varphi = (\varphi_+ - \varphi_-)$ serves as a conjugate coordinate. The phase space of this Hamiltonian has the topology of Bloch sphere. The Hamiltonian possesses two SPs that are located at $\tilde n = 0$ and $\tilde n = N$, which are the north and south poles of the Bloch sphere.

B. Trimer

The BHH for L sites in a ring geometry is

$$\mathcal{H} = \sum_{j=1}^{L}\left[\frac{U}{2}a_j^\dagger a_j^\dagger a_j a_j - \frac{K}{2}(e^{i(\Phi/L)}a_{j+1}^\dagger a_j + \text{H.c.})\right], \qquad (4)$$

where j mod(L) labels the sites of the ring, and other notations are as in the dimer case. The so-called Sagnac phase Φ is proportional to the rotation frequency of the device: it can be regarded as the Aharonov-Bohm flux that is associated with Coriolis field in the rotating frame [23,26].

It is convenient to switch to momentum representation. One defines annihilation and creation operators b_k and $b_k^\dagger$, such that $b_k^\dagger = \frac{1}{\sqrt{L}}\sum_j e^{ikj}a_j^\dagger$ creates bosons in the kth momentum orbitals. Here we consider a three-site ring that has three momentum orbitals labeled by their wave number $k = 0, 1, 2$. Later we assume, without loss of generality, that the particles are initially condensed in the $k = 0$ orbital. This is not necessarily the ground-state orbital, because we allow the possibility that the ring is in a rotating frame. After some time the condensate can be partially depleted such that the occupation is $(N-n_1-n_2, n_1, n_2)$.

Since we have here an effectively two freedom system, it is convenient to define relative phases $q_1 = \varphi_1 - \varphi_0$ and

$q_2 = \varphi_2 - \varphi_0$. Consequently the Hamiltonian can be written in terms of canonical coordinates as (Appendix A)

$$\mathcal{H}(\varphi, n; \phi, M) = \mathcal{H}^{(0)}(\varphi, n; M) + [\mathcal{H}^{(+)} + \mathcal{H}^{(-)}]. \quad (5)$$

Here $n = (n_1 + n_2)/2$ and $M = (n_1 - n_2)/2$, while the conjugate angle variables are $\varphi = q_1 + q_2$ and $\phi = q_1 - q_2$. The first term $\mathcal{H}^{(0)}$ is an integrable piece of the Hamiltonian that has M as an additional constant of motion:

$$\mathcal{H}^{(0)}(\varphi, n; M) = \mathcal{E}n + \mathcal{E}_\perp M - \frac{U}{3}M^2 + \frac{2U}{3}(N-2n) \times \left[\frac{3}{4}n + \sqrt{n^2 - M^2}\cos(\varphi)\right], \quad (6)$$

where U is the interaction between the bosons, while the detuning $\mathcal{E}$ determines the energy difference between the condensate ($n = 0$) and the depleted states ($n = N/2$). If we linearized $\mathcal{H}$ with respect to the (n_1, n_2) occupations, we would get the Bogoliubov approximation, which is Eq. (6) without the third term (M^2), and with $(N-2n) \approx N$. The additional terms $\mathcal{H}^{(\pm)}$ induce resonances that spoil the integrability, and give rise to chaos,

$$\mathcal{H}^{(\pm)} = \frac{2U}{3}\sqrt{(N-2n)(n\pm M)}(n\mp M)\cos\left(\frac{3\phi \mp \varphi}{2}\right). \quad (7)$$

Note that classically the total number of particles N can be removed from the Hamiltonian by a simple scaling of n and M. But upon quantization $1/N$ effectively plays the role of $\hbar$. It follows that the coherent state that is formed by condensation of the particles into a single orbital is represented in phase space by a Gaussian-like distribution of uncertainty width $1/N$. See for example [9,10]. The significance of this $1/N$ scale for the analysis of instabilities due to nonlinear resonances has been illuminated in [5].

III. STABILITY, GEOMETRY, AND TOPOLOGY

Considering the dimer Hamiltonian Eq. (1) it is well known that condensation at one orbital is always *stable*, while condensation at the second orbital becomes *unstable* if U is large enough. This conclusion can be arrived at by inspection of Eq. (3) : Without loss of generality let us assume that U is positive (or else the energy axis should be flipped); Considering condensation in the upper $(-)$ orbital, we can regard $\tilde{n} \equiv n_+$ as the depletion coordinate; then it follows, using the standard stability analysis of Appendix B, that the north pole ($\tilde{n} = 0$) becomes unstable if $|\mathcal{E}| < NU$.

Considering the trimer Hamiltonian, the superficial impression is that $\mathcal{H}^{(0)}$ of Eq. (6) is very similar to Eq. (3) of the dimer: all we have to do is to rescale the occupation coordinate $\tilde{n} = 2n$. However, the stability analysis of Appendix B shows that the regime diagram of Eq. (6) is in fact more interesting: the condensate ($n = 0$) is unstable for $-7NU/6 < \mathcal{E} < NU/6$, while the depleted state ($n = N/2$) is unstable for $-NU/6 < \mathcal{E} < 7NU/6$. We will focus, in particular, on the the range $|\mathcal{E}| < (1/6)NU$, where both SPs become unstable. Note that $n = 0$ necessary means that $M = 0$, while $n = N/2$ is a SP for all M values.

A. Geometry

The stability analysis reflects the algebraic side of the dynamics, but ignores the geometrical aspect. The phase space of the dimer is the Bloch sphere. All the $(\tilde{\varphi}, \tilde{n}{=}0)$ points are in fact the same point, which can be regarded as the north pole of the sphere. The same applies to $(\tilde{\varphi}, \tilde{n}{=}N)$ which can be regarded as the south pole of the sphere.

But for our three-site ring Eq. (6) the geometry of phase space is different. The south pole is no longer a single point, because different φ values indicate different points in phase space. So in fact we no longer have a Bloch sphere, but rather we have a Bloch disc. Another difference is that the angle is folded ($\varphi = 2\tilde{\varphi}$). The phase-space structure, for different values of the detuning, is illustrated in Fig. 2. The origin and perimeter of the (φ, n) disc should be identified with the north and south poles of the $(\tilde{\varphi}, \tilde{n})$ Bloch sphere. The origin ($n = 0$), if unstable, Figs. 2(b)–2(e), is the cusp on a folded separatrix of half-saddle topography. The perimeter of the disc is a *spread SP*. If the spread SP becomes unstable, Figs. 2(c)–2(f), there is a separatrix that comes out from the perimeter in an angle φ_{out}, and comes back to it in an angle φ_{in}. Both the approach and the departure from the perimeter along the separatrix require an extremely long time. We emphasize again that from an algebraic point of view the dynamics is the same as if the perimeter were a single point on a Bloch sphere. In the Bloch sphere each phase-space point is duplicated. Thanks to this duplication the separatrices that are associated with the SPs take the familiar figure-8 saddle shape, which is more illuminating for illustration purposes.

B. Topology

So far we have discussed the one-freedom projected dynamics of (φ, n). But now we have to remember that there is an additional degree of freedom (ϕ, M). We consider the dynamics that is generated by $\mathcal{H}^{(0)}$, where M is a constant of motion, and the conjugate angle is doing circles with $\dot{\phi} = \partial\mathcal{H}^{(0)}/\partial M$. A trajectory that is generated by $\mathcal{H}^{(0)}$ covers a torus in phase space. A useful way for visualizing the tori is based on the SU(1, 1) symmetry [19,27] of $\mathcal{H}^{(0)}$. The (φ, n) dynamics is the intersection of constant E and constant M surfaces; see Fig. 3 and Appendix C. In particular the $M = 0$ surface is a cone, whose tip corresponds to $n = 0$, while its outer boundary corresponds to $n = N/2$. If the intersection forms a closed loop, as in Fig. 3(a), the trajectory covers a torus in phase space. But if the trajectory goes through $n = 0$, as in Fig. 3(b), we get a *pinched torus*; see Fig. 3(c). This is because the ϕ circle at $n = 0$ has zero radius. This "zero radius" is explained as follows: if $n = 0$ then necessarily $n_1 = n_2 = 0$, hence all the (φ, ϕ) angles degenerate, representing a single phase-space point. In the projected dynamics Fig. 2, the cusped trajectory which goes through $n = 0$ (when unstable) is merely a projection of the pinched torus.

C. Definition of β

Consider a trajectory that has a period T in (φ, n). For illustration this can be the trajectory that loops along the intersection in Fig. 3(a). Clearly, this trajectory is in general not a closed loop in the full phase-space representation. Rather

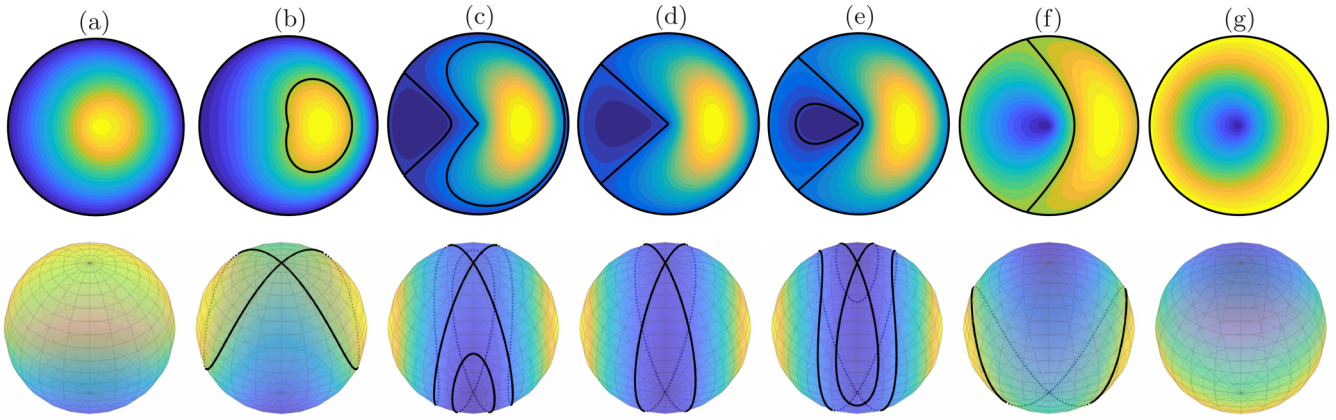

FIG. 2. The geometry of the projected phase space. Top panels: the (φ, n) disc. Bottom panels: the $(\tilde{\varphi}, \tilde{n})$ Bloch sphere. The detuning for (a)–(g) is $\mathcal{E}/NU = -4/3, -1/3, -0.05, 0, 0.05, 1/3, 4/3$. The color stands for the energy of $\mathcal{H}^{(0)}$, with $M = 0$. Black lines indicate the separatrices that go through the SPs.

it winds on a two-dimensional torus. We define β as the change in ϕ during time T. For a trajectory that passed through an unstable SP we have $T \to \infty$, and β is ill defined. In Fig. 1(a), we plot β as a function of M and E.

IV. SWAP TRANSITION

Recall that $\mathcal{E}$ is controlled experimentally by the rotation frequency of the device. Figure 2 shows the projected dynamics for different values of the detuning $\mathcal{E}$. In panels (c)–(e) both SPs are unstable, and we see how they *swap* as the detuning changes sign. At the transition the two separatrices coalesce, thus forming a connection between the origin $n = 0$ (which supports the condensate) and the perimeter $n = N/2$ (where the $k = 0$ orbital is completely depleted).

On the Bloch sphere, both north and south poles, when unstable, take the familiar 8-like shape. As we previously argued, this is due to the fact that the phase space is duplicated, and that all the φ values at the south pole are regarded as a single point. This physically unfaithful presentation possibly better reflects what we mean by "swap of separatrices." We note that the Poincaré sections in [10], that had been presented before we gained proper understanding of the swap transition, were physically unfaithful in the same sense.

Once the $\mathcal{H}^{(\pm)}$ terms are added, a connecting quasistochastic strip is formed, through which the initial state can decay.

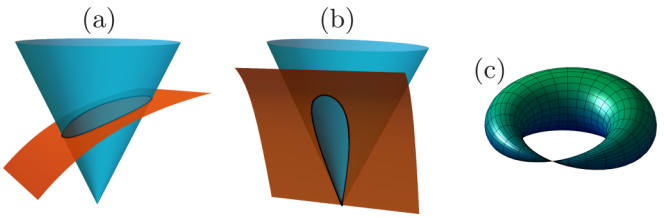

FIG. 3. Phase-space topology. The blue cone is an $M = 0$ surface, that intersects with a surface of constant E. The existence of an additional coordinate (ϕ) at each point is implicit. The intersection is a torus. Panel (a) is the typical case, while (b) corresponds to a pinched torus (see text). The latter is fully illustrated (with ϕ) in panel (c).

This is shown in Fig. 4, where we plot a Poincaré section of the full Hamiltonian Eq. (5). One should note the subtle relation between the perspective of Fig. 4 and that of Fig. 2. A panel of the latter displays sections of $M = 0$ tori that form a vertical subset in a Fig. 1–type (M, E) diagram, while a panel of Fig. 4 displays sections of the same E trajectories that form a horizontal subset of such diagram. The pinched torus is contained in both subsets.

Away from the swap transition, the chaotic region around $n = 0$ is bounded by the surviving Kolmogorov-Arnold-Moser (KAM) tori, forming a *chaotic pond* which is isolated from the perimeter region. Hence the depletion of the condensate is arrested. It is only in the vicinity of the swap transition that a connected chaotic pathway to depletion is

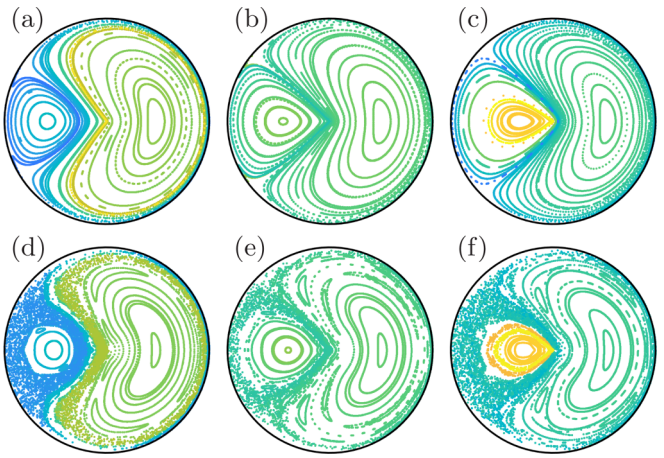

FIG. 4. Poincare sections. The dynamics of the full Hamiltonian Eq. (5) projected to the (φ, n) disc. All the trajectories are launched with the same energy as that of the condensate, and the section is chosen to be $q_2 = 0$. The left to right arrangement of the panels is by detuning $\mathcal{E}/NU = -0.05, 0, 0.05$, in one-to-one correspondence with Figs. 2(c)–2(e). In the upper panels the interaction strength is $NU \sim 1$, in units of the BHH hopping frequency K, while in the lower panels it is doubled, keeping $\mathcal{E}/NU$ fixed. The color code (from yellow to blue) corresponds to the trajectory-averaged occupation n (from $N/8$ to $N/2$).

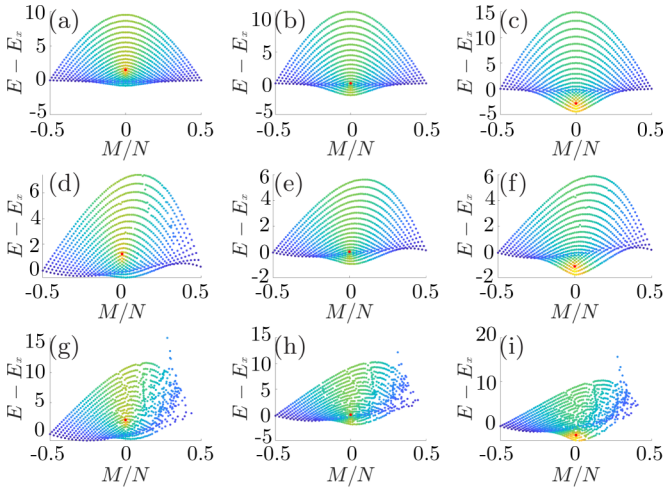

FIG. 5. The spectrum. The left to right arrangement of the panels is as in Fig. 4. In the upper row we plot the spectrum of $\mathcal{H}^{(0)}$, while the two other rows provided the spectrum of $\mathcal{H}$ in one-to-one correspondence with Fig. 4. All the spectra refer to ring with $N = 42$ particles. The points are colored by the expectation value of n, with the same color code as in Figs. 1(b) and 4.

formed. Thus, a local stability analysis of the SP using the standard Bogoliubov procedure does not provide the proper criterion for superflow metastability.

V. QUANTIZATION

The classical structure of phase space is reflected in the many-body spectrum. If chaos is ignored the eigenstates can be labeled by the good quantum numbers that are determined by the commuting operators M and $\mathcal{H}^{(0)}$, as in Fig. 1(b). If we add the $\mathcal{H}^{(\pm)}$ terms we can still order the energies according to the expectation value $\langle M\rangle$. Several examples are provided in Fig. 5. For presentation purpose, the perimeter energy $E_x(M)$, which corresponds to maximum depleted state $(n = N/2)$, is taken as the reference. Figure 7 of Appendix D provides spectra for the whole range of the detuning parameter, corresponding to the phase-space plots of Fig. 2.

From a semiclassical perspective, if we ignore the chaos, each point can be associated with an EBK torus; see Appendix E. Namely, the "good quantum numbers" are quantized values of the action variables. The lattice arrangement of the energies in Fig. 1(b) reflects the way that the tori are embedded in phase space, while the chaos, once added, blurs it locally; see Fig. 5. This lattice arrangement is supported by a classical skeleton that is formed by a pinched torus (marked by a red dot), and an $E = E_x(M)$ separatrix. At the vicinity of the separatrix the spectrum is dense, reflecting that the frequency of the motion goes to zero. Irrespective of that, the quantum spectrum has a topological defect that is described by a monodromy (to be further discussed below). This monodromy reflects the presence of the pinched torus. The sequence of panels in Fig. 5 shows how the swap transition is reflected in the quantum spectrum. This transition happens as the red dot, which corresponds to the pinched torus, crosses the $E = E_x$ separatrix line. We see how the yellow condensation region is diminished at the transition.

VI. MONODROMY CALCULATION

The concept of monodromy is pedagogically summarized in Appendix E. For our model system, in the absence of chaos, we have in involution the generators $H_1 = \mathcal{H}^{(0)}$ and $H_2 = M$. The trajectories that are generated for a given E and M form a torus. Any point on the torus is accessible by generating a walk of duration (t_1, t_2). Consider the projected dynamics in (φ, n). A given trajectory has a period T, but in the full phase space it is, in general, not periodic, because ϕ has advanced some distance β. It follows that in order to get a periodic walk on the torus, the $t_1 = T$ evolution that is generated by H_1 should be followed by a $t_2 = -\beta$ evolution that is generated by H_2. The so-called rotation angle β characterizes the torus, and is imaged in Fig. 1(a). Note that a $t_2 = 4\pi$ evolution that is generated by $H_2 = M$ is a periodic trajectory in phase space, because it does not affect the (φ, n) degree of freedom. We conclude that the set of periodic walks forms a lattice that can be spanned by the basis vectors

$$\vec{\tau}_a = (T, -\beta), \tag{8}$$

$$\vec{\tau}_b = (0, 4\pi). \tag{9}$$

A remark is in order regarding the determination of the 4π in Eq. (9). It should be clear that the original phases $(\varphi_0, \varphi_1, \varphi_2)$ are defined mod (2π). Next we define the coordinates $q_1 = \varphi_1 - \varphi_0$ and $q_2 = \varphi_2 - \varphi_0$, and the alternate coordinates $\phi = q_1 - q_2$ and $\varphi = q_1 + q_2$. If the alternate coordinates are regarded as mod (2π) angles, it follows that each (φ, ϕ) represents *two* points in q space, and each (φ, n) in our sections is the projection of a 4π circle. Consider a trajectory that is generated using $H_2 = M$. In the (φ_1, φ_2) torus it will have a constant φ. You would have to run t a 4π interval in order to get back to the starting point.

Quantum to classical duality

Let us now go back to Fig. 1(a), where we plot β as a function of M and E. One can immediately spot the location of the pinched torus $(M, E) = 0$, around which β has 4π variation. Hence, after a parametric loop, we get the mapping $\vec{\tau}_a \mapsto \vec{\tau}_a - \vec{\tau}_b$ while $\vec{\tau}_b$ remains the same. Such nontrivial mapping is the hallmark of monodromy [11,12]. Upon EBK quantization monodromy in the spectrum is implied; see Appendix E. This is demonstrated in the inset of Fig. 1(b). Namely, transporting an elementary unit cell (spanned by two basis vectors) around the pinched torus in the (M, E) spectrum, we end up with a different unit cell.

In Fig. 1(a) the detuning was chosen such that the SP at $n = N/2$ is stable. Contrary to that, in Fig. 5 the detuning is such that the SP is at the vicinity of a swap transition. Consequently the spectrum is divided into two regions by the separatrix line, and only the region with the pinched torus exhibits the nontrivial monodromy. At the swap transition the pinched torus and hence the nontrivial monodromy is relocated to the other region. In the special case of $\mathcal{E} = 0$, the pinched torus merges with the separatrix line, leaving both regions with a trivial monodromy.

VII. SUMMARY

Several themes combine in the study of superflow metastability. There is a monodromy that is associated with the SP that supports the condensate, and a separatrix that is associated with an SP that folds all the depleted states. The two SPs determine the skeleton of phase space. By duality it is also the skeleton for the many-body quantum spectrum (via EBK quantization). In the Bloch sphere representation (Fig. 2) the two SPs look alike, but this is in fact wrong and misleading. The topological distinction between the central SP and the peripheral SP becomes conspicuous once we look on the quantum spectrum where the central SP-monodromy appears as a topological defect that reflects the existence of a pinched torus, while the depleted peripheral states form a dense line in (M, E) space.

By itself the above described skeleton is not enough for the understanding of BEC metastability or its absence. The theoretical narrative requires the fusion of *chaos* into the story. If the rotation frequency of the device is adjusted (which controls the detuning between the central SP and the peripheral separatrix), a stochastic pathway is formed at the "swap transition," leading to the depletion of the condensate, and the decay of the superflow. In the dual quantum picture chaos blurs the ordered spectrum. Away from the swap transition the topological aspect remains robust, but at the swap transition eigenstates get mixed and become ergodic within the stochastic region.

The analysis that we have introduced is specifically relevant for future hysteresis-type experiments [23] with ring lattice circuits [28,29]. Furthermore, the trimer is not only the minimal model for ergodization due to chaos, it is also the minimal configuration for thermalization [30], and serves as the building block for progressive thermalization of large arrays [31,32]. Finally, it should be recognized that the theme of metastability is of general interest for mathematical physics studies of high dimensional chaos, irrespective of specific application.

ACKNOWLEDGMENTS

This research was supported by the Israel Science Foundation (Grant No. 283/18).

APPENDIX A: TRIMER HAMILTONIAN

For a clean L-site ring lattice we define momentum orbitals whose wave numbers are $k = (2\pi/L) \times$ integer. Consequently the BHH takes the form

$$\mathcal{H} \;=\; \sum_{k} \epsilon_k b_k^\dagger b_k \;+\; \frac{U}{2L} {\sum_{k_4 k_3 k_2 k_1}}' b_{k_4}^\dagger b_{k_3}^\dagger b_{k_2} b_{k_1}, \qquad \text{(A1)}$$

where the constraint $k_1+k_2+k_3+k_4 = 0 \bmod(2\pi)$ is indicated by the prime, and $\epsilon_k = -K\cos(k-\Phi/L)$ are the single-particle energies. Later we assume, without loss of generality, that the particles are initially condensed in the $k = 0$ orbital. This is not necessarily the ground-state orbital, because we keep Φ as a free parameter. Note that below and in the main text we optionally use k as a dummy index to label the momentum orbitals.

For the $L = 3$ site ring we have

$$\mathcal{H} = \sum_{k=0,1,2} \epsilon_k n_k \;+\; \frac{U}{6}\sum_k n_k^2 \;+\; \frac{U}{3}\sum_{k'\neq k} n_{k'} n_k \;+\; \frac{U}{3}\sum_{k''\neq k'\neq k} [n_{k'} n_{k''}]^{1/2}\, n_k \,\cos\left(\varphi_{k''}+\varphi_{k'}-2\varphi_k\right). \qquad \text{(A2)}$$

We define $q_1 = \varphi_1 - \varphi_0$ and $q_2 = \varphi_2 - \varphi_0$ where the subscripts refer to $k_{1,2} = \pm(2\pi/3)$. Using the notation $\mathcal{E}_k = (\epsilon_k - \epsilon_0) + (1/3)NU$ we get Eq. (5) with

$$\mathcal{H}^{(0)} = \mathcal{E}_1 n_1 + \mathcal{E}_2 n_2 \;-\; \frac{U}{3}\left[n_1^2 + n_2^2 + n_1 n_2\right] + \frac{2U}{3}(N - n_1 - n_2)\sqrt{n_1 n_2}\cos\left(q_1 + q_2\right) \qquad \text{(A3)}$$

and

$$\mathcal{H}^{(+)} = \frac{2U}{3}\sqrt{(N-n_1-n_2)n_1}\; n_2 \cos\left(q_1 - 2q_2\right) \qquad \text{(A4)}$$

while $\mathcal{H}^{(-)}$ is obtained by swapping the indices $(1 \leftrightarrow 2)$. In fact it is more convenient to use the coordinates

$$\begin{aligned} \phi[\mathrm{mod}(4\pi)] \;&=\; q_1 - q_2 \;=\; \varphi_1 - \varphi_2, \\ \varphi[\mathrm{mod}(2\pi)] \;&=\; q_1 + q_2 \;=\; \varphi_1 + \varphi_2 - 2\varphi_0 \end{aligned} \qquad \text{(A5)}$$

and the conjugate coordinates

$$M \;=\; \frac{1}{2}(n_1 - n_2) \;\in\; \left[-\frac{N}{2}, \frac{N}{2}\right], \qquad \text{(A6)}$$

$$n \;=\; \frac{1}{2}(n_1 + n_2) \;\in\; \left[|M|, \frac{N}{2}\right]. \qquad \text{(A7)}$$

Then the Hamiltonian takes the form of Eq. (5) with Eqs. (6) and (7), where the detuning is $\mathcal{E} = \mathcal{E}_1 + \mathcal{E}_2 - (1/2)NU$, and $\mathcal{E}_\perp = \mathcal{E}_1 - \mathcal{E}_2$.

APPENDIX B: SPS AND SEPARATRICES

Consider a phase space that is described by φ, n. We shall distinguish between *rotor geometry* for which the $n = 0$ points are distinct, and *oscillator geometry* for which all the $n = 0$ points are identified as one point. The algebraic treatment is the same, but the physical interpretation is different.

1. Regular point

As an appetizer consider the Hamiltonian

$$H \;=\; \sqrt{2n}\sin(\varphi). \qquad \text{(B1)}$$

It looks singular at $n = 0$, but in fact it is completely smooth there. Regarded as an oscillator it is canonically equivalent to $H = p$ that generates translations. Similar observation applies to the noninteracting dimer Hamiltonian $H = (1/2)(a_2^\dagger a_1 + \text{h.c.})$, which in action angle variables takes the form

$$H \;=\; \sqrt{\left(\frac{N}{2} - n\right)\left(\frac{N}{2} + n\right)}\;\cos(\varphi). \qquad \text{(B2)}$$

Here both the north and south poles of the Bloch sphere $(n = \pm N/2)$ are regular phase-space points, neither SP nor singular.

2. Stationary point

Consider the standard quadratic Hamiltonian $H = (1/2)[ap^2 + bx^2]$. In polar canonical coordinates it is

$$H = [A + B\cos(2\varphi)]n \tag{B3}$$

with $A = (a + b)$ and $B = (a - b)$. If $ab > 0$, equivalently $|A| > |B|$, the origin ($n = 0$) is an elliptic SP that is circled by trajectories that have the frequency

$$\omega = \sqrt{ab} = \sqrt{A^2 - B^2}. \tag{B4}$$

Otherwise the origin becomes an unstable hyperbolic SP. In the latter case there is an 8-like separatrix that goes through the origin: there are two ingoing directions and two outgoing directions. The approach to the SP along the separatrix, and its departure, is an infinitely slow motion. The SPs of the dimerEq. (3) are described locally by the above Hamiltonian.

3. Folded SP

Consider the dimer Hamiltonian Eq. (3) with $2\tilde{\varphi}$ replaced by φ. Here the dynamics is the same from an algebraic perspective, but the global geometry is different. It is a folded version of the dimer Hamiltonian. In the hyperbolic case the vicinity of the SP can be described as "half saddle." From local dynamics point of view the equations of motion are identical, but here the separatrix has only one outgoing direction and only one ingoing direction.

4. Spread SP

Consider Eq. (B3), but assume that we are dealing with rotor geometry. From a local dynamics point of view the equations of motion are still identical, but now the arrival point (say φ_{in}) and the departure point (say φ_{out}) are not the same point.

5. Stability analysis

Consider the Hamiltonian of Eq. (6) with $M = 0$. The origin ($n = 0$) is a *folded SP*. It is elliptic or hyperbolic depending on the detuning. Locally the Hamiltonian looks like Eq. (B3) with

$$A = \mathcal{E} + \frac{NU}{2}, \quad B = \frac{2NU}{3}, \tag{B5}$$

$$\text{SP unstable for } -\frac{7NU}{6} < \mathcal{E} < \frac{NU}{6}. \tag{B6}$$

In the regime where the SP is stable the ω of Eq. (B4) reflects the frequency of the Bogoliubov excitations [10]. In the hyperbolic case we have a separatrix that goes through the origin.

For the same Hamiltonian, the perimeter ($n = N/2$) is a *spread SP*. For the purpose of stability analysis we can identify the points along the perimeter as a single point of a Bloch sphere. Setting $\tilde{n} = N - 2n$ the Hamiltonian looks like Eq. (B3) with

$$A = -\frac{\mathcal{E}}{2} + \frac{NU}{4}, \quad B = \frac{NU}{3}, \tag{B7}$$

$$\text{SP unstable for } -\frac{NU}{6} < \mathcal{E} < \frac{7NU}{6}. \tag{B8}$$

In the hyperbolic case we have a separatrix that meets the perimeter at one point and departs in a different point. Combining with Eq. (B6) we see that both SPs are unstable if $|\mathcal{E}| < (1/6)NU$. In the latter case we have two separatrices. The separatrices swap as we go through $\mathcal{E} = 0$; see Fig. 1.

6. Case of nonzero M

For the same Hamiltonian Eq. (6) with $M \neq 0$, the points along the inner boundary $n = M$ are distinct. So we cannot regard them as a single point. Close to this inner boundary we have $H \sim \sqrt{\tilde{n}}\cos(\varphi)$, with $\tilde{n} = n - M$. This is a nonsingular Hamiltonian, essentially the same as Eq. (B1), that generates regular flow. It follows that the inner boundary is not special from a dynamical point of view: it can be regarded as *spread regular point*, it is not an SP, and there is no separatrix there.

The stability of the perimeter is determined as in Eq. (B8), but with B multiplied by $\sqrt{1 - (2M/N)}$. Therefore, for sufficiently large M we always have $|A| > |B|$ and the perimeter is stable.

APPENDIX C: CONICAL INTERSECTION PERSPECTIVE

A useful way for visualizing the phase-space tori is based on the SU(1, 1) symmetry [19,27] of $\mathcal{H}^{(0)}$. For that we express the two conserved quantities, namely the energy E and the constant of motion M, in terms of the group generators. We start by introducing

$$K_z = n + \frac{1}{2}, \quad K_+ = a_1^\dagger a_2^\dagger, \quad K_- = a_1 a_2, \tag{C1}$$

which is a realization of the SU(1, 1) group, satisfying the algebra

$$[K_z, K_\pm] = \pm K_\pm, \quad [K_+, K_-] = -2K_z. \tag{C2}$$

The Casimir operator of the group, which commutes with all the generators, is

$$C = K_z^2 - K_x^2 - K_y^2, \tag{C3}$$

where K_x and K_y are given by $K_\pm = K_x \pm iK_y$. In the semiclassical treatment we have

$$K_x \sim \sqrt{n_1 n_2}\cos\varphi \in [-\Delta, \Delta], \tag{C4}$$

$$K_y \sim \sqrt{n_1 n_2}\sin\varphi \in [-\Delta, \Delta], \tag{C5}$$

$$K_z \sim n \in \left[|M|, \frac{N}{2}\right], \tag{C6}$$

where $\Delta = \sqrt{(N/2)^2 - M^2}$. The Hamiltonian can be written in terms of the generators as

$$\mathcal{H}^{(0)} = \mathcal{E}K_z + \mathcal{E}_\perp M - \frac{U}{3}M^2 + \frac{2U}{3}(N - 2K_z)\left[\frac{3}{4}K_z + K_x\right]. \tag{C7}$$

As for the constant of motion M, we have $M^2 = C$. In Fig. 6 we plot several examples for the M^2 and $\mathcal{H}^{(0)} = E$ surfaces in the (K_x, K_y, K_z) space. For $M = 0$ Eq. (C3) defines a cone whose tip corresponds to $n = 0$, while its outer boundary corresponds to $n = N/2$. For for a constant $M \neq 0$ Eq. (C3)

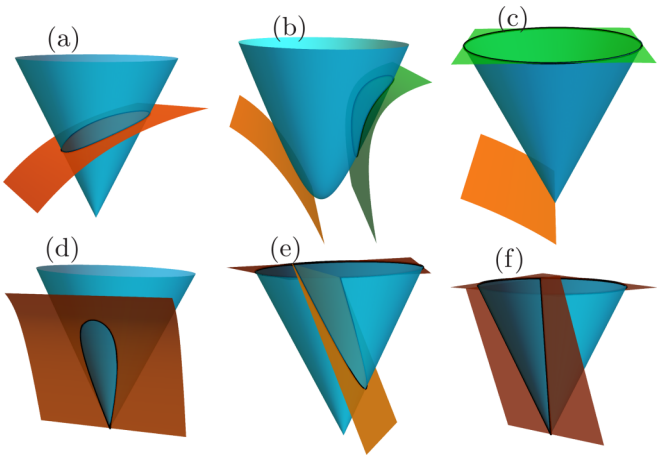

FIG. 6. Several examples of the reduced phase space in the (K_x, K_y, K_z) coordinates (the symmetry axis is K_z). The blue cone (a),(c)–(f) is the surface of constant $M = 0$ while the blue hyperbole (b) is the surface of constant $M = 0.15N$. The remaining surfaces correspond to a constant E. The intersection of constant M and E surfaces (highlighted in black) is a trajectory in the reduced (φ, n) space, and provides a useful way of visualizing the phase-space tori (see text).

defines a hyperboloid whose base corresponds to $n = |M|$, while its outer boundary corresponds to $n = N/2$.

The intersection between the E and M^2 surfaces is a trajectory in the reduced (φ, n) phase space. In the full phase space, we also have the phase ϕ, which dynamically changes as $\dot{\phi} = \partial\mathcal{H}^{(0)}/\partial M$. If the intersection between the surfaces forms a closed loop, as in Figs. 6(a) and 6(b), the dynamics in the full (φ, ϕ, n, M) phase space covers a two-torus (which is, of course, the typical case in an integrable two degrees of freedom system). When the two surfaces are tangent, as in Fig. 6(b), the trajectory is a fixed point in the (φ, n) space, and a circle in the full phase space.

Trajectories that pass through $n = 0$ should be addressed with more caution. As explained in the main text, the tip of the cone does not correspond to a ϕ circle, but to a single point. This is because $n = 0$ means $n_1 = n_2 = 0$ so that ϕ is degenerate. When the $n = 0$ SP is stable, the energy surface is tangent to the tip of the cone, as in Fig. 6(c), hence the trajectory is a single point in phase space. When unstable, the intersection forms a cusped circle, see Fig. 6(d), representing a *pinched torus*, i.e., a torus with one of its ϕ circles shrinks to a point.

Trajectories that pass through $n = N/2$ are special too. When the $n = N/2$ SP is stable, as in Fig. 6(c), the intersection is the entire outer circle of the cone, reflecting the fact that it is a *spread* SP. When unstable, see Fig. 6(e), a separatrix trajectory is formed, which meets the $n = N/2$ circle at two points, corresponding to $\varphi_{\rm in}$ and $\varphi_{\rm out}$. At the swap transition, the two SPs are connected, i.e., the cusped circle of $n = 0$ merged with the separatrix trajectory of $n = N/2$, as shown in Fig. 6(f).

APPENDIX D: GALLERY

Here we provide additional plots of the spectra for the whole range of the detuning parameter. Figure 7 is an extended version of Fig. 5 and corresponds to Fig. 2.

APPENDIX E: HAMILTONIAN MONONDROMY

Consider generators (H_1, H_2) in involution, i.e., that commute with each other. The generated trajectories are moving on an energy surface labeled (E_1, E_2). A *walk* consists of t_1 evolution using H_1, and t_2 evolution using H_2. The involution implies that the walks are commutative. Accordingly the parametrization of a walk is $\vec{t} = (t_1, t_2)$. A periodic walk is a walk that brings you back to the same point. The set of periodic walks forms a lattice in $\vec{t}$ space. This lattice is spanned by basis vectors $\vec{\tau}_k$, where $k = a, b$. We can formally write any point in $\vec{t}$ space as

$$\vec{t} \;=\; \sum_k \frac{\theta_k}{2\pi}\vec{\tau}_k = \frac{\theta_a}{2\pi}\vec{\tau}_a + \frac{\theta_b}{2\pi}\vec{\tau}_b. \tag{E1}$$

We define a reciprocal basis such that

$$\vec{\omega}_k \cdot \vec{\tau}_{k'} = 2\pi\delta_{k,k'}. \tag{E2}$$

The reciprocal relation is

$$\theta_k = \vec{\omega}_k \cdot \vec{t}. \tag{E3}$$

Once action variables are defined we have

$$\vec{\omega}_k = \left(\frac{\partial H_1}{\partial J_k}, \frac{\partial H_2}{\partial J_k}\right). \tag{E4}$$

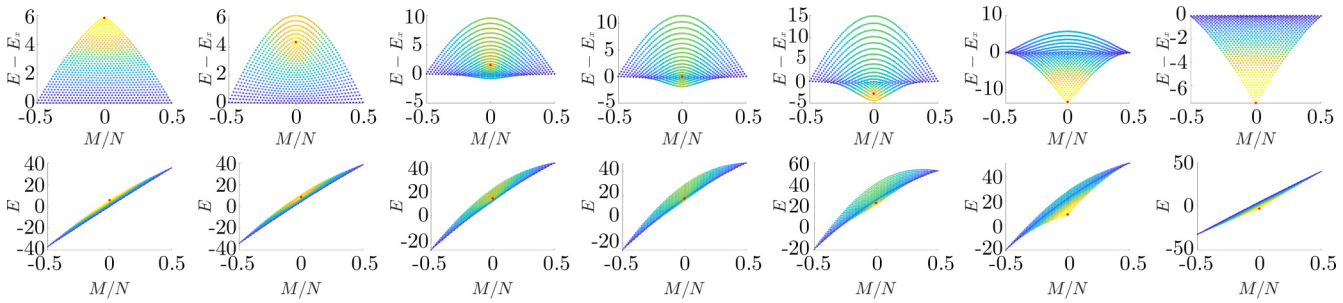

FIG. 7. The spectrum. The top row panels are the spectra of $\mathcal{H}^{(0)}$ with the same $\mathcal{E}/NU$ values as in Fig. 2. In the bottom row the same spectra are plotted, but without subtracting the separatrix energy. The interaction strength from left to right is $NU \approx 0.2, 0.6, 1.4, 1.9, 2.7, 1.9, 0.3$ in units of the BHH hopping frequency K. Note that for the top row panels, different NU values will produce the same plot and only scale the E-E_x axis. Note that the energy here differs by a constant from Fig. 1(b).

The spacings between two energies is

$$\Delta E = \sum_k \vec{\omega}_k \cdot \overrightarrow{\Delta n}_k, \tag{E5}$$

Thus the spectrum forms a reciprocal lattice.

Considering a closed loop in (E_1, E_2) space, the monodromy matrix is defined as the mapping

$$\vec{\tau}_k(\text{final}) = \sum_l \mathbf{M}_{kl} \vec{\tau}_l. \tag{E6}$$

If the loop encircles a pinched torus we have [12]

$$\mathbf{M} = \begin{pmatrix} 1 & -1 \\ 0 & 1 \end{pmatrix} \tag{E7}$$

so we get the mapping $\vec{\tau}_a \mapsto \vec{\tau}_a - \vec{\tau}_b$, as discussed in the main text after Eq. (8). For the reciprocal basis we have

$$\vec{\omega}_k(\text{final}) = \sum_l \tilde{\mathbf{M}}_{kl}\, \vec{\omega}_l, \tag{E8}$$

where $\tilde{\mathbf{M}} = [\mathbf{M}^{-1}]^t$. This can be seen by writing

$$\begin{aligned} 2\pi\, \delta_{k,k'} &= [\vec{\omega}_k(\text{final})] \cdot [\vec{\tau}_{k'}(\text{final})] \\ &= \sum_{lm} \tilde{\mathbf{M}}_{kl} \mathbf{M}_{k'm}\, \vec{\omega}_i \cdot \vec{\tau}_j = 2\pi \sum_l \tilde{\mathbf{M}}_{kl} \mathbf{M}_{k'l} \end{aligned} \tag{E9}$$

hence $\tilde{\mathbf{M}}\mathbf{M}^t = \mathbf{1}$ and $\tilde{\mathbf{M}} = [\mathbf{M}^{-1}]^t$. For a loop which encircles the pinched torus we then have

$$\tilde{\mathbf{M}} = \begin{pmatrix} 1 & 0 \\ 1 & 1 \end{pmatrix}, \tag{E10}$$

which reflects the way $\vec{\omega}_k$ are mapped, and therefore how a unit cell in the quantum spectrum is transformed, as seen in Fig. 1(b).

[1] M. Chuchem, K. Smith-Mannschott, M. Hiller, T. Kottos, A. Vardi, and D. Cohen, Quantum dynamics in the bosonic josephson junction, Phys. Rev. A **82**, 053617 (2010).

[2] M. Albiez, R. Gati, J. Fölling, S. Hunsmann, M. Cristiani, and M. K. Oberthaler, Direct Observation of Tunneling and Nonlinear Self-Trapping in a Single Bosonic Josephson Junction, Phys. Rev. Lett. **95**, 010402 (2005).

[3] S. Levy, E. Lahoud, I. Shomroni, and J. Steinhauer, The ac and dc josephson effects in a bose–einstein condensate, Nature (London) **449**, 579 (2007).

[4] L. Amico, D. Aghamalyan, F. Auksztol, H. Crepaz, R. Dumke, and L. C. Kwek, Superfluid qubit systems with ring shaped optical lattices, Sci. Rep. **4**, 04298 (2014).

[5] G. Arwas and D. Cohen, Superfluidity in Bose-Hubbard circuits, Phys. Rev. B **95**, 054505 (2017).

[6] Gh.-S. Paraoanu, Persistent currents in a circular array of bose-einstein condensates, Phys. Rev. A **67**, 023607 (2003).

[7] D. W. Hallwood, K. Burnett, and J. Dunningham, Macroscopic superpositions of superfluid flows, New J. Phys. **8**, 180 (2006).

[8] A. Gallemí, M. Guilleumas, J. Martorell, R. Mayol, A. Polls, and B. Juliá-Díaz, Fragmented condensation in Bose–Hubbard trimers with tunable tunnelling, New J. Phys. **17**, 073014 (2015).

[9] A. R. Kolovsky, Bose-Hubbard hamiltonian: Quantum chaos approach, Int. J. Mod. Phys. B **30**, 1630009 (2016).

[10] G. Arwas, A. Vardi, and D. Cohen, Superfluidity and chaos in low dimensional circuits, Sci. Rep. **5**, 13433 (2015).

[11] J. J. Duistermaat, On global action-angle coordinates, Commun. Pure Appl. Math. **33**, 687 (1980).

[12] R. H. Cushman and L. M. Bates, *Global aspects of classical integrable systems*, Vol. 94 (Springer, Basel, 1997).

[13] R. Cushman and J. J. Duistermaat, The quantum mechanical spherical pendulum, Bull. Am. Math. Soc. **19**, 475 (1988).

[14] S. Vũ Ngoc, Quantum monodromy in integrable systems, Commun. Math. Phys. **203**, 465 (1999).

[15] B. Zhilinskii, Hamiltonian monodromy as lattice defect, in *Topology in Condensed Matter*, edited by M. I. Monastyrsky (Springer, Berlin, Heidelberg, 2006), pp. 165–186.

[16] K. Efstathiou, M. Joyeux, and D. A. Sadovskií, Global bending quantum number and the absence of monodromy in the HCN ↔ CNH molecule, Phys. Rev. A **69**, 032504 (2004).

[17] R. H. Cushman, H. R. Dullin, A. Giacobbe, D. D. Holm, M. Joyeux, P. Lynch, D. A. Sadovskií, and B. I. Zhilinskií, CO_2 Molecule as a Quantum Realization of the 1 : 1 : 2 Resonant Swing-Spring with Monodromy, Phys. Rev. Lett. **93**, 024302 (2004).

[18] N. J. Fitch, C. A. Weidner, L. P. Parazzoli, H. R. Dullin, and H. J. Lewandowski, Experimental Demonstration of Classical Hamiltonian Monodromy in the 1 : 1 : 2 Resonant Elastic Pendulum, Phys. Rev. Lett. **103**, 034301 (2009).

[19] A. Lamacraft, Spin-1 microcondensate in a magnetic field, Phys. Rev. A **83**, 033605 (2011).

[20] M. Kloc, P. Stránský, and P. Cejnar, Monodromy in dicke superradiance, J. Phys. A: Math. Theor. **50**, 315205 (2017).

[21] H. R. Dullin and H. Waalkens, Defect in the Joint Spectrum of Hydrogen due to Monodromy, Phys. Rev. Lett. **120**, 020507 (2018).

[22] M. P. Nerem, D. Salmon, S. Aubin, and J. B. Delos, Experimental Observation of Classical Dynamical Monodromy, Phys. Rev. Lett. **120**, 134301 (2018).

[23] S. Eckel, J. G. Lee, F. Jendrzejewski, N. Murray, C. W. Clark, C. J. Lobb, W. D. Phillips, M. Edwards, and G. K. Campbell, Hysteresis in a quantized superfluid 'atomtronic' circuit, Nature (London) **506**, 200 (2014).

[24] O. Morsch and M. Oberthaler, Dynamics of Bose-Einstein condensates in optical lattices, Rev. Mod. Phys. **78**, 179 (2006).

[25] I. Bloch, J. Dalibard, and W. Zwerger, Many-body physics with ultracold gases, Rev. Mod. Phys. **80**, 885 (2008).

[26] A. L. Fetter, Rotating trapped Bose-Einstein condensates, Rev. Mod. Phys. **81**, 647 (2009).

[27] M. Novaes, Some basics of su (1, 1), Rev. Bras. Ensino Fis. **26**, 351 (2004).

[28] T. A. Bell, J. A. P. Glidden, L. Humbert, M. W. J. Bromley, S. A. Haine, M. J. Davis, T. W. Neely, M. A. Baker, and H. Rubinsztein-Dunlop, Bose-Einstein condensation in large time-averaged optical ring potentials, New J. Phys. **18**, 035003 (2016).

[29] M. Aidelsburger, J. L. Ville, R. Saint-Jalm, S. Nascimbène, J. Dalibard, and J. Beugnon, Relaxation Dynamics in the Merging of n Independent Condensates, Phys. Rev. Lett. **119**, 190403 (2017).

[30] I. Tikhonenkov, A. Vardi, J. R. Anglin, and D. Cohen, Minimal Fokker-Planck Theory for the Thermalization of Mesoscopic Subsystems, Phys. Rev. Lett. **110**, 050401 (2013).

[31] D. M. Basko, Weak chaos in the disordered nonlinear Schroedinger chain, Ann. Phys. **326**, 1577 (2011)

[32] H. Hennig and R. Fleischmann, Nature of self-localization of Bose-Einstein condensates in optical lattices, Phys. Rev. A **87**, 033605 (2013).